Physical properties of HfO₂ nano structures deposited using PLD

Evan T. Salim[1,*], Ahmed T. Hassan[2], Rana O Mahdi[1], Forat H. Alsultany [3]

[1]Applied Science Department, University of Technology, 10066 Baghdad, Iraq
[2]Ministry of Education, Directorate General for Education, Baghdad Al-Karkh/1
[3]Al-Mustaqbal University College, Department of Medical Physics, Iraq

ABSTRACT

On Quartz substrates, high purity transparent conductive the Di-Oxide of the (HfO₂) Nano and micro-structure films were successfully coated. The method of (PLD) Deposition using Pulsed Laser, and the influence of laser energy was investigated. The XRD results revealed two distinct phases, cubic and monoclinic crystal shapes. Peaks in the Fourier-transform infrared (FTIR) spectra showed that HfO₂ nanofilm was forming.The findings of the optical characteristics reveal an excellent transparency of nearly 80% (89 percent). As the laser wavelength decreases, the optical energy band gap values for Nanostructure of HfO₂ were prepared, with values ranging from 5.24 to 5.53 eV. Also, the EDX results showed the appearance of hafnium peaks and oxygen peaks in varying proportions, which confirms that hafnium oxide is definitely obtained The results of the AFM reveal that when the pulsed laser intensity increases, the average grain diameter values increase from 52.96 to 74.54 nm. With regard to optimum pulsed laser energy, the based on I-V characterization, the generated factor ideality for created diodes was discovered to be decreasing, and the corresponding values of the barrier height grew. The ideality factor of the diode made the optimum pulsed laser energy (1800 mJ) was greater (n=3.1).

Keywords: PLD; structural properties; Optical properties; HfO₂; optical band gap

1. INTRODUCTION

The (HfO₂) Nano Hafnium oxide nanostructures is one of the most popular significant optical and photonic materials will be coated, because of the good ranges of the optical constants like the refractive index and broad transparency values ranging from UV wavelengths around 250 nanometers to MIR wavelengths around 1200 nanometers [1–5].

Nano HfO2 monoclinic structure has an optical energy bandgap of roughly 5.6 eV, whereas the infrared phonons those are active has a frequency of less than 8000 mm-1 [6–9]. Due to electrical properties such as high refractive index, optical bandgap, and dielectric constant values, as well as the finest stability of the chemical, i.e. excellent process's compatibility with ongoing IC technology, hafnium dioxide has been reported as a compete with a many other high (k dielectrics), such as titanate of zirconium, titanate of the barium-strontium, and others. Several optical applications for a nano and micro structures of the hafnium dioxide have previously been discovered, including various kinds of coatings that reduce glare (anti-reflection of the coatings), (coatings of visible, coating NIR, and coating mid IR) [3, 10-14], as well as various types of mirrors (filters band-pass, and mirrors chirped) [4], mirrors (UV) at a high threshold for harm [6], and finally a windows with energy-saving, thermal mirrors [15].

---

* Corresponding author: evan_tarq@yahoo.com, & evan.t.salim@uotechnology.edu.iq

Because of the best region of the constant (real-dielectric) (εr≈23) and strong chemical stability, there have been significant and concentrated investigations and the studies on the feasibility of employing (HfO$_2$) the hafnium oxide as a silicon oxide alternative in the production of optoelectronics, optical gated and the electrical devices [16–20].

Furthermore, because to a high point for the melting of the Nano hafnium oxide films and the high values of the thermal stabilities [21], Various Nanomaterials based on hafnium show potential as thermal barriers for turbine blades working in high-temperature and severe environments. [22, 23]. Deposition aided by plasma ions [1, 6, 7, 24], Deposition of chemical vapors [9, 25], deposition using the solution chemical [26, 27], evaporation with an ion beam [10], plating with reactive ions [10, 28], laser deposition using pulses [13, 29], Deposition using an electron beam [30-31], and RF sputtering [32-34] have all been used to deposit Nanostructures of the hafnium oxide under various preparation conditions [35, 36].

2. Experimental process

Figure 1 depicts the part of the experimental for laser deposition using pulses (PLD) process (1). The Q-switching (Nd: YAG) laser was utilized in the PLD system, and the major parameters were shown in the table (1). The Joule-meter of Genetic type QE12 was used to calibrate the energy of the employed laser.

Figure 1. System for the Deposition of the Pulsed Laser

Table 1 The parameter that used for deposition

Pulsed Laser Parameters	Values
Laser Wavelengths	0.532 μm
Energy of the Pulses	1600, 1700, and 1800 mj
Pulse duration	10ns
Frequency of Pulses per second	3 Hz
Temperatures of the Substrate	350 C$^{\text{o}}$

Using a Q-switching Nd: YAG laser with a wavelength of 532 nm and a laser energy range of 1600-1800 mj, 200 pulses were produced. The deposition using pulsed laser experiment was carried out in a chamber of vacuum under the setting of a value for vacuum of 1 atm (10-2Torr).

The employed laser beams were focused at a 45-degree angle on the target. The Nano films were formed on quartz substrates at 350°C and varied laser energies of 1600-1800 mj, using wavelength of pulsed laser of 532 nm.

The employed target is made using a very high quality pellet of the Nano-powder of HfO_2 are (99.99%) from Gamma company and is formed like a thick disk with a diameter of around 1.5 cm and a width (thickness) of 0.5 cm before the deposition procedure.

The morphological, structural, and optical characteristics of the measured thickness of manufactured and prepared Nano-film has been studied utilizing a variety of measuring methods, including X-Ray diffraction, Scanning Electron Microscopy, and Atomic Force Microscopy studies. Following the deposition of hafnium dioxide nanofilms, the generated samples were examined and evaluated, with structural parameters assessed using an XRD (X-Ray diffraction) system (X'Pert Pro MRD PW3040) utilizing Cu-K radiation at 0.15418 nm wavelength. Fourier-Transform infrared (FTIR) spectroscopy from (BRUKER-7613) was utilized to examine the bonds of HfO_2.

The optical results were tested using (UV-Vis Shimadzu, model No: 1800 from Japan). The surface topography for the produced Nanofilms was evaluated using two types of tests: the Scanning Prop Microscope (SEM Shimadzu, SPM-9600, "Japan"), and also its used to test the EDX, finally an AFM test using (JOEL-JSM'6460LV' AFM-9600, "Analytical Oxford" instruments Ltd. From Japan).

The current-voltage properties were measured using a Keithley Electrometer (Model No. 6517-B). On a silicon wafer (n-type, Si100) with a resistance of 0-30.cm and a thickness of 250 m, type $Al/HfO_2/n$-Si hetero-junction diodes were constructed. To form a contact, pure aluminium was sputtered on the deposited HfO_2/n-Si utilizing (dc sputtering) with a square mask 1X1 cm and a thickness of 200 nm.

3. Result and discussions

Figure 2 shows the results for XRD pattern of the Nanostructures of the Nano hafnium oxide films at various pulsed laser energies; the findings of the X-Ray show that a Nanostructure of the Nano hafnium oxide films be more crystallized as the energy of pulsed laser was increased as a result of increased the rate of the growing and deposition with the increasing the laser energy. In addition, two phases of hafnium dioxide were discovered in these results: hafnium oxide (cubic) and hafnium dioxide (monoclinic) [37-39]. Using the higher laser energy (1800 mj), a distinct rise in the values intensity of the (phase cubic) could be seen, which might be connected to an increase in laser beam energy, resulting in a powerful ablation process at this phase [40, 41].
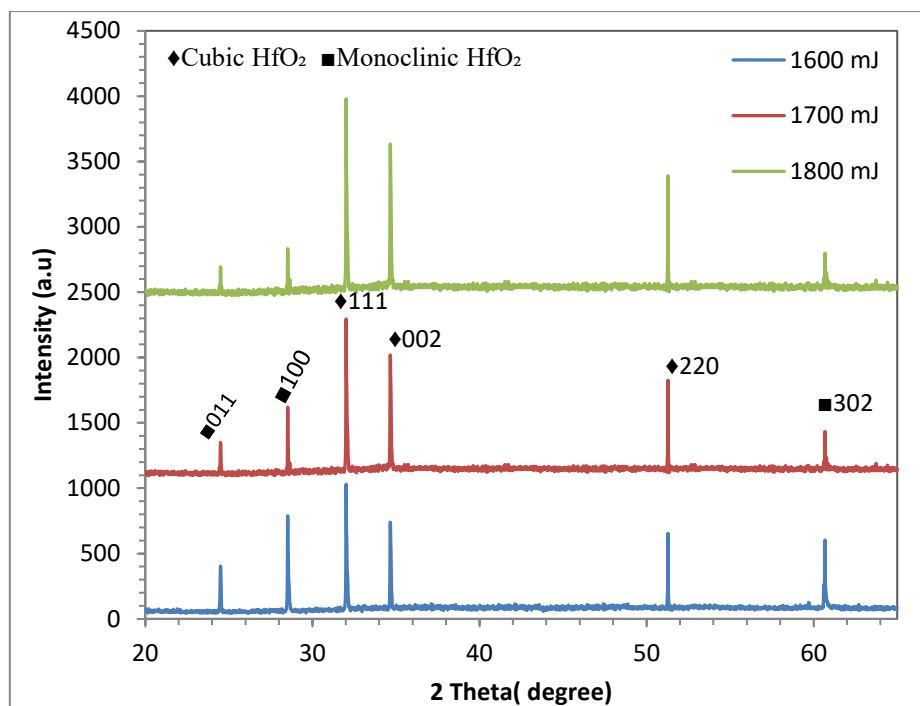
Figure 2. XRD patterns of HFO$_2$ Nanostructures deposited using various Laser energies.

The created Nano-hafnium oxide has been chemically analysed using Fourier Transform Infrared (FTIR) spectroscopy to determine the existence of different bonds and if each bond vibrates at a particular frequency. The 430 to 3930 cm^{-1} wavelength ranges were used to capture the FT-IR spectra. In Figure 3, the distinctive peaks at 761, 672, and 513 cm^{-1} were attributed to the Hf-O vibrational mode of HfO$_2$; Additionally, the vibrational mode of crystalline HfO$_2$ is in the IR (800-400 cm^{-1}) active phonon mode range [19]. These peaks precisely coincide with previously published theoretical estimates of monoclinic HfO$_2$ [24]. The absorption frequency measured at 1613 cm^{-1} , 1633 cm^{-1}, and 1339 cm^{-1} (Figure 3) is attributed to the bending vibration of the H-O-H bond and the bidentate carbonate symmetric stretching, respectively. These findings were mostly consistent with those seen in the previously published literature [25]. The purity of the produced HfO$_2$ nanoparticles is confirmed by the lack of extra peaks in FT-IR spectra.
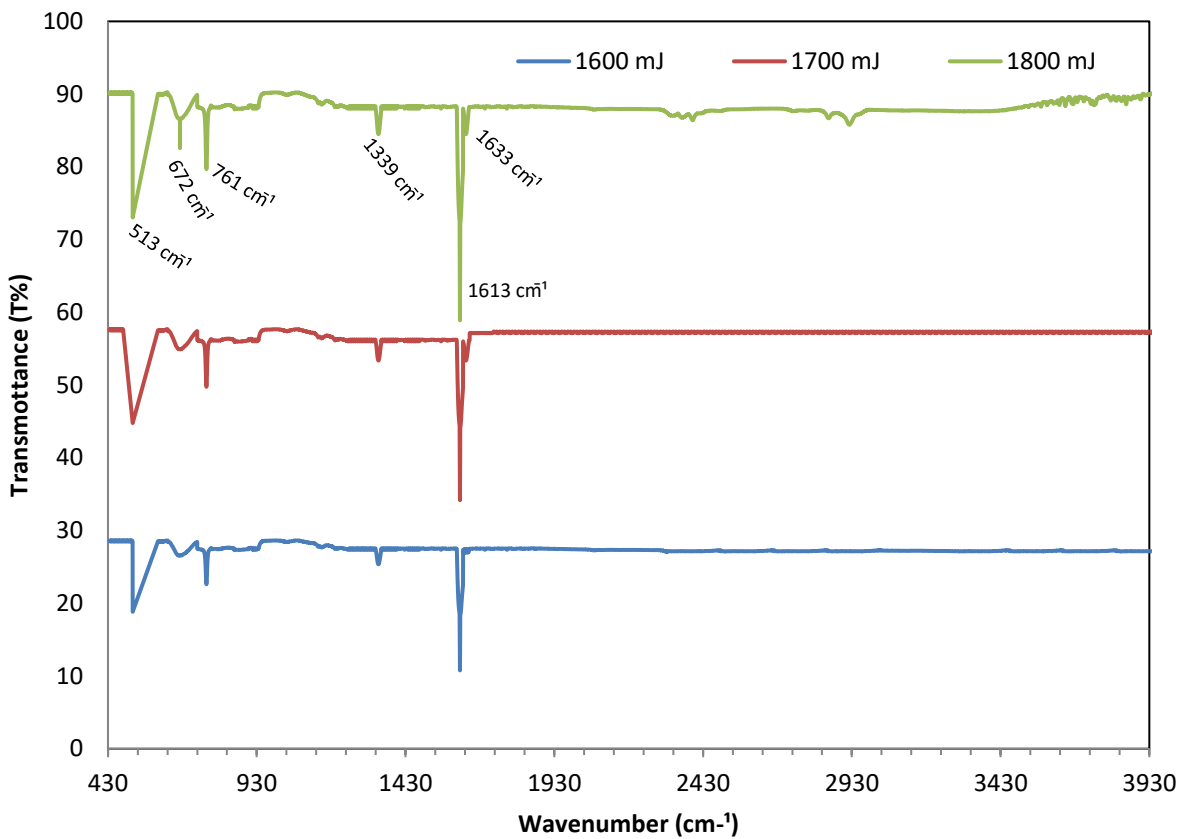
Figure 3. FTIR patterns of HFO_2 Nanostructures deposited using various Laser energies.

Using an optical reflectometer instrument, Figure 4 shows the changes in the thickness values of the created Nanostructures at various lasers energy. The utilization of the second harmonic generation can reveal a distinct rise in Nano-film thickness [42-44]. This rise implies that the positive sizes of grains modifications that deform the surface to make it more smooth have a favorable relationship. It is obvious that a value of the thicknesses is increasing from 128 nm at 1600 mj to 177 nm at 1700 mj, and 193 nm at 1800 mj as result of increasing the deposition and growing rate.
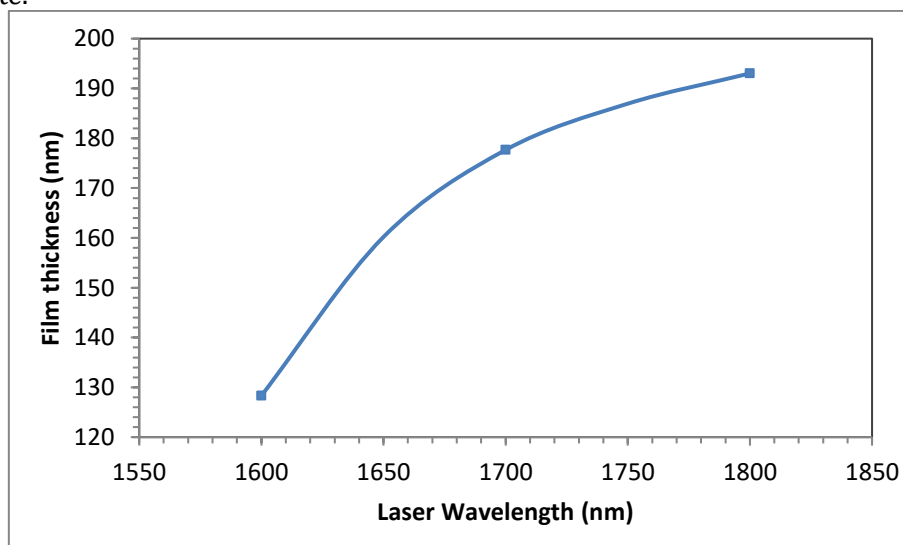
Figure 4. Thickness do Nano-films for HFO_2 deposited using various Laser energies.

Figure 5 shows the spectrum for the absorption for prepared the Nano hafnium oxide films at various energies of pulsed laser. These numbers are examined based on the transmission numbers. The absorption values were enhanced as laser energies, with the findings showing a steady increasing in absorption values as the laser energy were increased, or in other words, the absorption value was increased as the deposition rate was increased [45-47]. This indicates that absorption levels are proportional to the laser's energy; the greater the laser's energy, the higher the absorption value. It is obvious those values of the optical absorption have dramatically fallen to values of less than 0.35 μm, and that the values of absorption increased with increased laser energy owing to a rise in the concentration of hafnium dioxide grains.
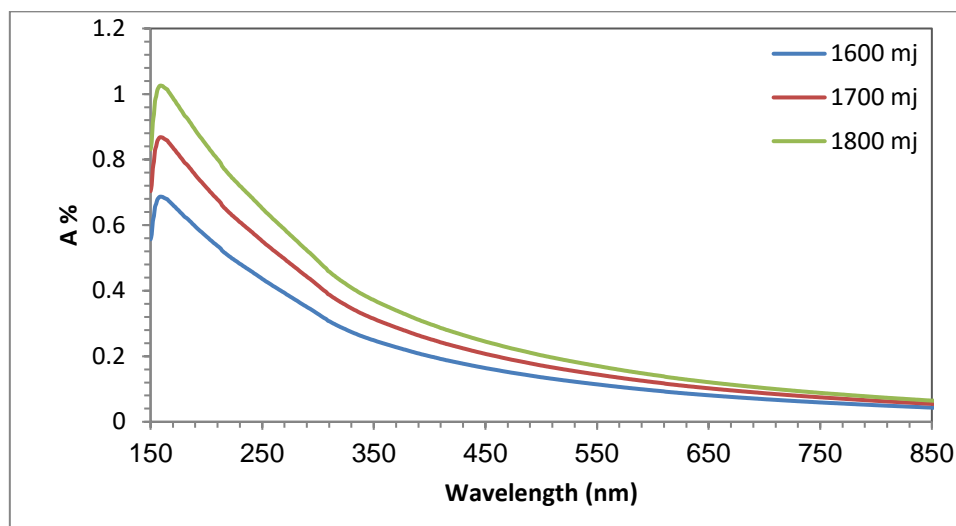
Figure 5. Absorbance spectra for Nano HFO_2 structures using various energies of laser.

The transmission T% percent spectra for Nano HfO_2 structure are shown in Figure 6. The values of coming too near with a 91.1 percent to 75.4 percent increase in optical transmission as the laser energy are changed from 1600, 1700, and 1800 mj, respectively. The low values of transmission for the region of UV, as a physical property of Nano hafnium oxide films, where the values of the transmission for hafnium oxide Nano-films are connected to the value of the energy band-gap at the region of UV. The high optical transmission value in the visible area range suggests that the Nano-films are extremely homogenous and have a low surface roughness value [48-50].

The optical transmission values was enhanced with the energies of pulsed laser, with the data indicating a constant reduced in the transmission values as the laser energy was raised, or in other words, the transmission value decreased as the deposition rate rose. That is to say, transmission levels are associated with energy of the pulsed laser; the lower the energy of the laser, the greater the transmission value. The optical transmission values are clearly lowered after passing the 350 nm threshold, and transmission is reduced with increased laser intensity due to an increase in hafnium dioxide grain concentration [51-53].
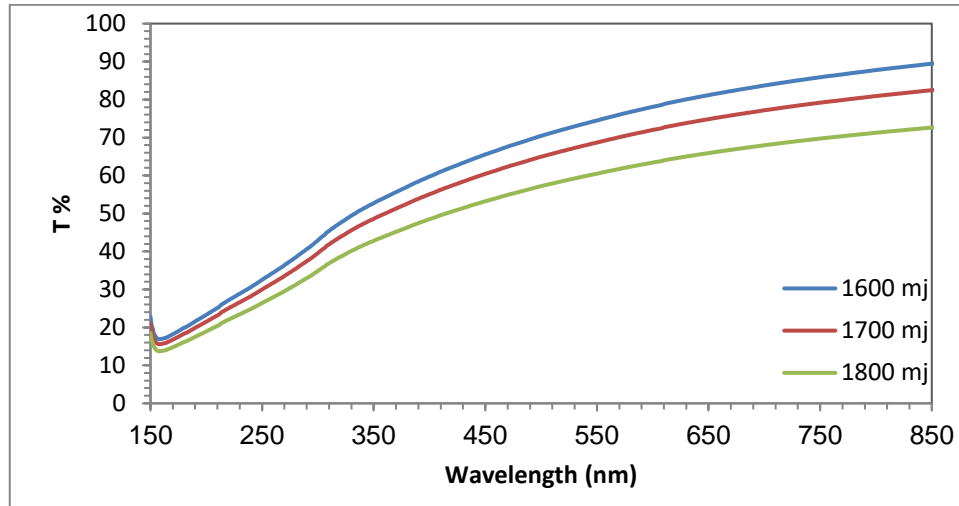
Figure 6. Transmittance spectra of Nano HFO$_2$ structure using various energies of laser.

Figure 7 shows the values of the optical bandgap for hafnium oxide Nano-films prepared using various energies of the pulsed laser; the values of energy band gap for HfO$_2$ Nanostructures ranged (5.02-5.52) eV. It is clear from these patterns that the optical band gaps increase with increasing laser energies; this is due to an increase in the rate of deposition and an improvement in the distribution of the structures [55-56].
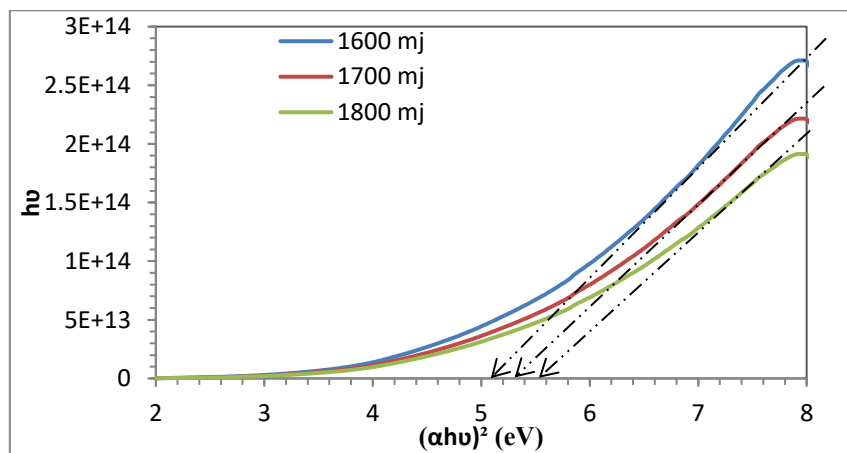
Figure 7. Optical energy band gab pattern for Nano HFO2 structure using various laser energies.

Figure 8 shows AFM images for the Nanostructures of hafnium oxide placed on substrates of quartz at various laser intensities. The photos show the surface composition, which includes the distribution and regular density for the prepared Nanostructures over the entire surface [57-58]. The images of the AFM show that the values diameter for average grains are inversely proportional to the laser energy employed. Where values of grains are 91.27 nm for energy of pulsed laser1600 mj, 58.63 nm for the laser energy 1700 mj, and the value of grains of 42.13 nm for the laser energy 1800 mj altered from (42.13–91.27) nm. Where it can be seen that as the laser energy increases, the value of energy band-gap for the formed nanostructure also rise [59-60]. The mean values of roughness's and the values RMS, values roughness fall as the pulsed laser energy rise, and the values of average roughness's decline from (0.2 to 10.45) nm as the energies of the pulsed laser decreases, while the values of the RM S decrease from (3.68 to 1.97) nm as the laser energies decrease. Table 2 calculates all constants' schedule for the surface below.

Table 2 average RMS values, diameters, and the average roughness's of Nanostructures of hafnium oxide at different energies of pulsed laser.

Energies of pulsed Laser (nm)	Number of Sample	RMS values (nm)	Roughness's values (nm)	Grains Diameter (nm)
1600	a	3.68	0.2	91.27
1700	b	2.44	6.65	58.63
1800	c	1.97	10.45	42.13

(a)   (b)

(c)
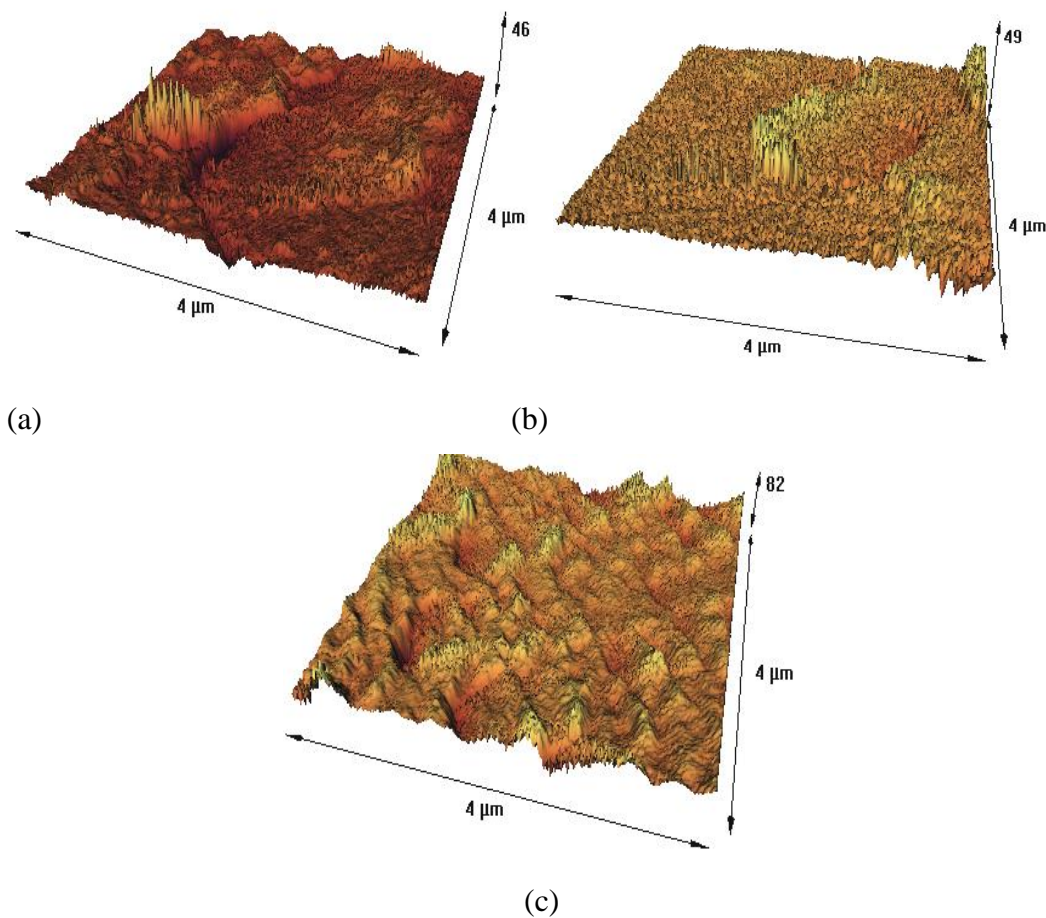
Figure 8. AFM images for Nano hafnium oxide structures prepared at various laser energies.

Figure 9 shows the grain size and roughness patterns for Hafnium dioxide, showing that the grain size of the deposited nanofilms decreased as the deposited laser energies increased, from 91.27 nm at 1600 mj to 42.13 nm at 1800 mj, while the surface roughness of the deposited nanofilms increased, as shown in the same figure.
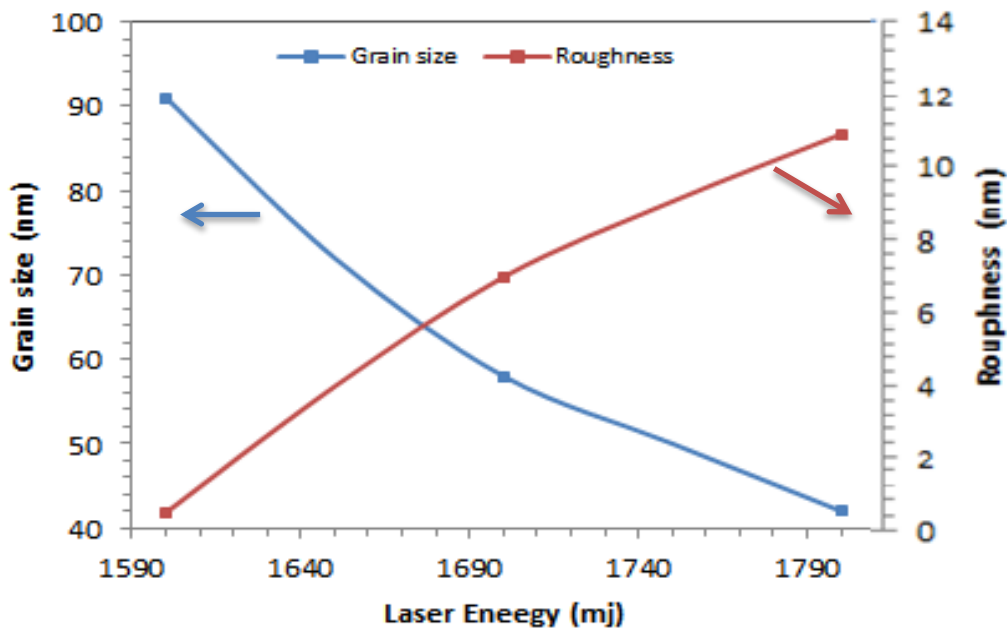
Figure 9. The grain size and the roughness of HFO$_2$ films at the different Laser energies.

Figure 10 displays images of SEM findings for hafnium dioxide Nanofilms created using the Pulsed Laser Deposition process at various deposited laser energies [61-63]. The grain size of the deposited hafnium dioxide nanofilms on quartz substrates is clearly influenced by the deposited laser energy. The Nano spherical grains are more distributed in the deposited Nanofilms of hafnium dioxide prepared with the laser energy of 1800 nm, as shown in Figure 10(a), and the average size of these particle sizes was about 45 nm, while the average size of the Nano spherical grains of hafnium dioxide prepared with the laser energy of 1600 nm was about 93 nm, as shown in Figure 10(b). These values of grain size reduction with high laser wavelength are due to an increase in deposited laser energy, which is connected to particle size reduction and increased deposition rate [64-66].
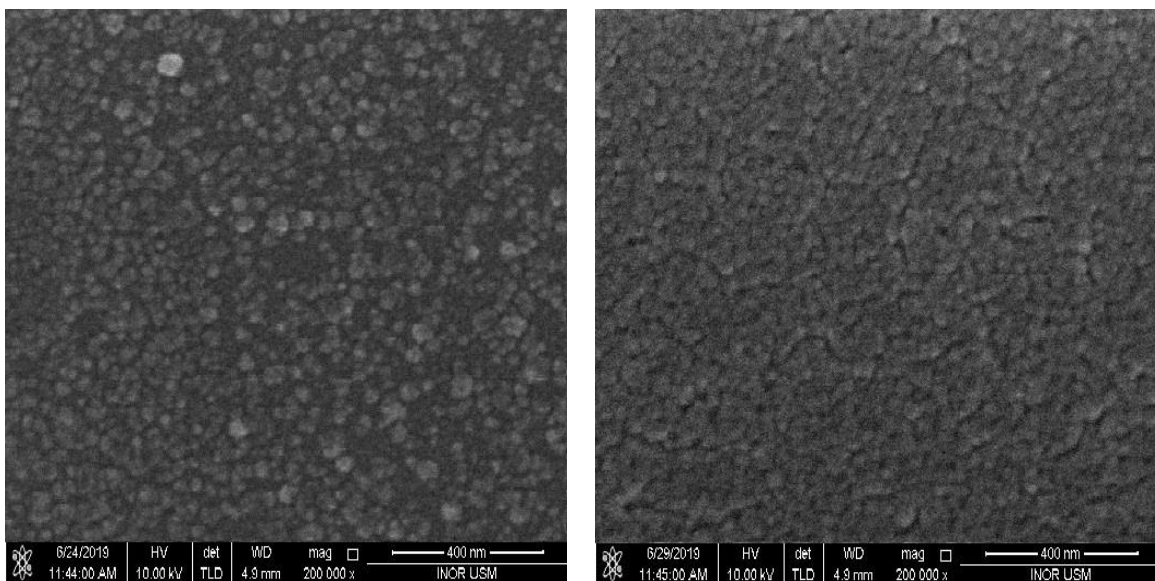
(a)   (b)

Figure 10. Images of the SEM for Nano HfO$_2$ films deposited at various laser energies.

The presence of hafnium oxide has been confirmed from EDX spectra. The EDX spectrum for the deposited hafnium oxide Nanofilms on the quartz substrates at the different Laser energies is presented in Figure 11, the data of EDX was found from the SEM samples. Due to a variety of factors such as Nano film thicknesses and the different energies of the pulsed laser, the ratios of the M and L peak heights for the three deposition parameters are different.

1600 mJ

1700 mJ

1800 mJ
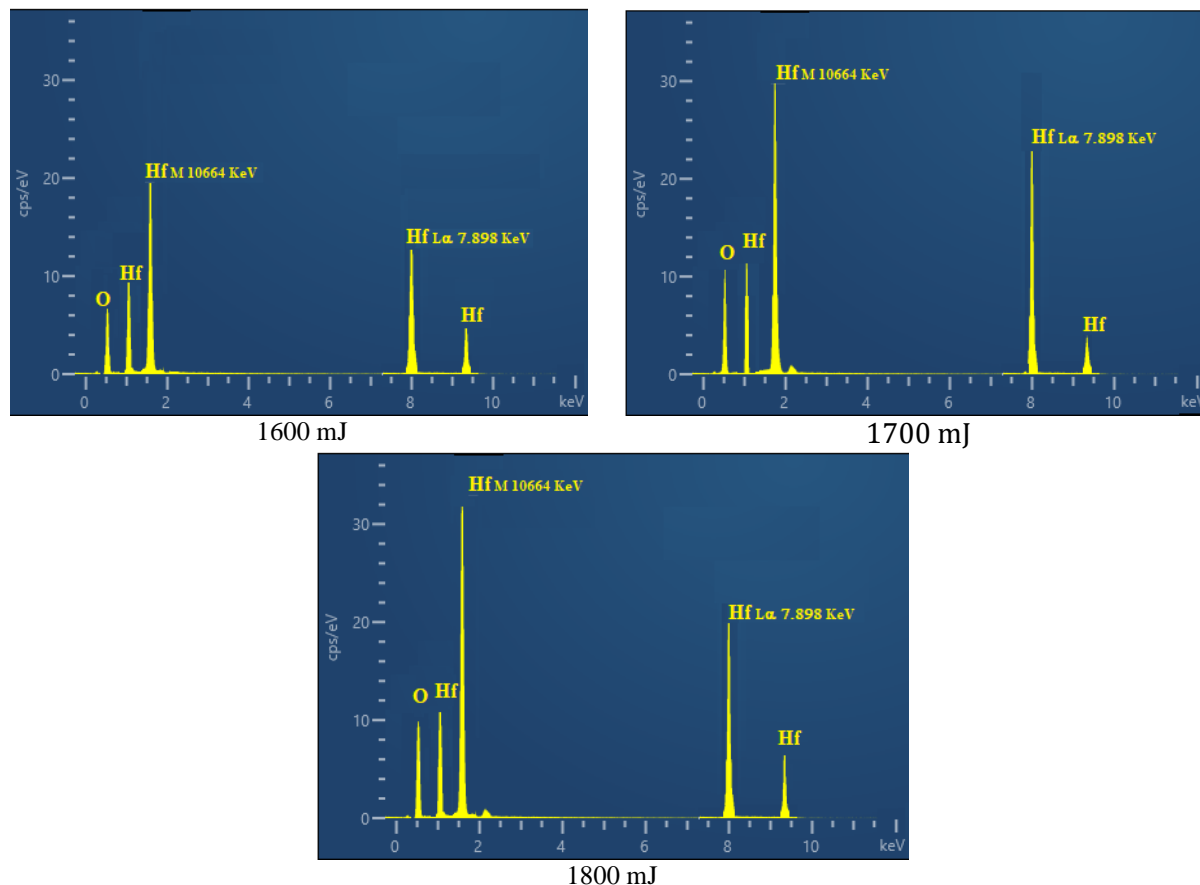
Figure 11. EDX result for Nano HfO₂ films deposited at various laser energies.

To build the optoelectronic device, a Hafnium dioxide Nanostructures layer was formed on the Si wafer P-type and a mask of Aluminum was deposited up to the HfO$_2$ nanostructure. Figure 12 shows the voltage-current (I-V) characterization of the deposited (Al/HfO$_2$/p-Si) at various pulsed laser energies. The findings of the I-V will be utilized to look at Schottky contacts, the quality interface, device performance, and limits. A constant biasing voltage ranging from -3 to +3 V was used to evaluate the reverse and forward current levels of the constructed device. The measured forward current develops exponentially with voltage for all of the manufactured diodes, indicating good rectification performance at 1800 mJ pulsed laser energy, reverse current is minimized, while forward current development is exponential, indicating increased rectification capabilities and the outstanding quality of the deposited and produced devices (diodes). A barrier Schottky is formed by contact/junctions (Metal-Semiconductor) MS and semiconductor hetero-junctions with similar configurations. An MS contact is also known as a Schottky diode. The bulk of charge carriers are in charge of carrier transit at these sites. To investigate the current transport mechanism in these devices, the current-voltage characteristics are evaluated across a large pulsed laser energy range. Using the thermionic-emission theory, the barrier height and ideality factor are calculated using the intercept and slope of the J-V curve (semi-logarithmic). According to the thermionic-emission theory, the current via Al/HfO₂/P-Si was calculated using the equations below. [67-69].

$$I = AA^*T^2 \exp\left(-\frac{q\Phi_B}{K_BT}\right)\left[\exp\left(\frac{qV}{nK_BT}\right) - 1\right] \tag{1}$$

The diode's reverse saturation current, I_0, was computed.

$$I_0 = AA^*T^2 \exp\left(-\frac{q\Phi_B}{K_BT}\right) \tag{2}$$

where I_0 denotes reverse saturation current, q denotes electron charge, V denotes bias voltage, n denotes ideality factor, B denotes effective barrier height, K_B denotes Boltzmann constant, T denotes temperature, A denotes diode area, and A^* denotes the constant of the effective barrier height. -Richardson. The I_0 value indicates reverse saturation current and minority carrier diffusion in the depletion area at forwarding bias and is a parameter of the manufactured diode. Among three based voltages, the value of the Io for the produced diode increases with pulsed laser energy, from $I_0 = 438.4.2$ mA at 1600 mJ to $I_0 = 857.1.5$ mA at 1800 mJ.
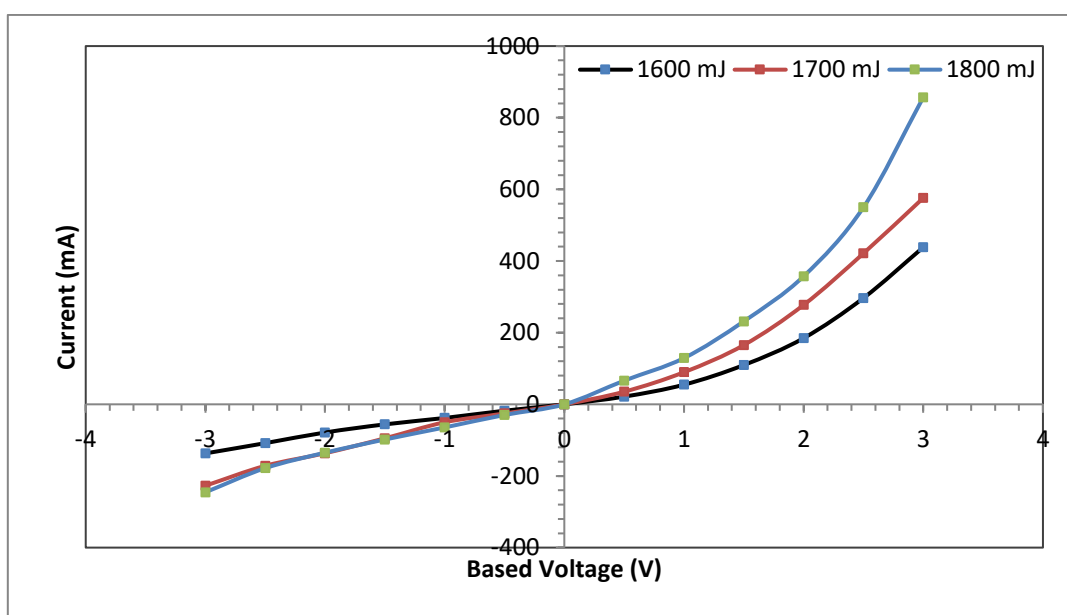
Figure 1. I-V characteristics of Al/HfO₂/p-Si barrier hetero-structure devise
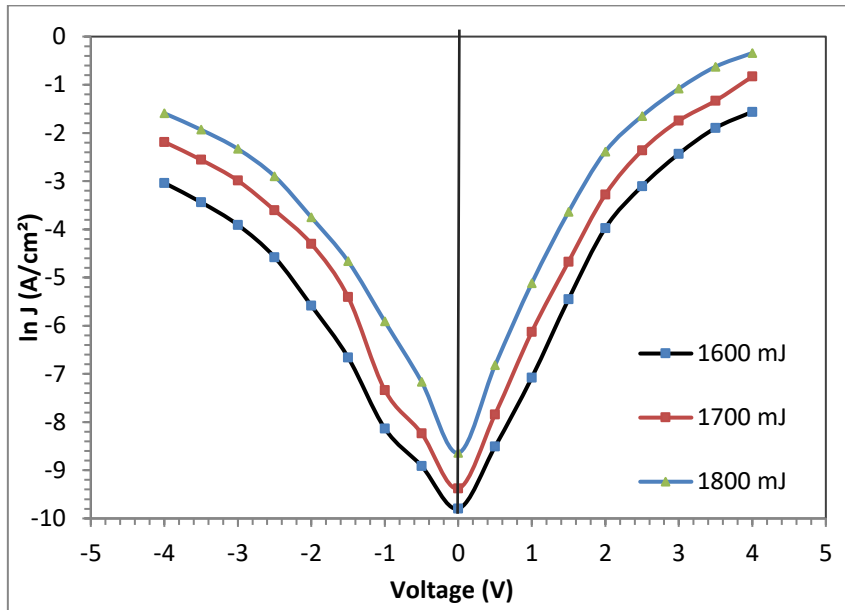
Figure 2. Density of Current (ln J) with the applied voltage (V) for the fabricated device

The forward bias slopes and intercept were determined using the ln J vs. voltage plot (Figure 13) and the following equation to predict the Al/HfO$_2$/p-Si diodes' ideal factors (n) and barrier heights (experimental values) [70-73].

$$n = \frac{q}{k_B T}\left(\frac{d(V)}{d(\ln(I))}\right) \tag{3}$$

$$\Phi_B = \frac{K_B T}{q}\ln\left(\frac{AA^* T^2}{I_0}\right) \tag{4}$$

The computed values of the factor (ideality) were calculated to be lowering as the pulsed laser powers increased, and the corresponding height barrier was growing. The electrons can overcome the lower value of the barriers or patches at the lowest value of the pulsed laser intensity. As a result, current transport will be dominated by values flowing through patches with lower barrier height and a higher ideality factor. More electrons have enough energy to break through the greater barrier as the pulsed laser intensity increases. The height of the barrier will climb as the pulsed laser energy rises in this case [74, 75]. At 1800 mJ pulsed laser energy, the Al/HfO$_2$/p-Si diode has a minimum (ideality) factor of 3.1, which corresponds to a barrier height of B = 0.789 eV. The smaller the n, according to Altndal et al. and Harishsenthil et al., the higher the B value at maximum pulsed laser intensity. [75, 76]. A number of research groups have also reported pulsed laser energy dependent Schottky diodes manufactured with various approaches [76, 77]. Many research have detailed the dependent-temperature based on the Schottky device created using various approaches. [77, 78]. The electron does not have enough energy to pass through the barrier energy at minimum pulsed laser energy due to the thermionic emission sample; nevertheless, at the maximum pulsed laser energy, the greater values of barriers are easily overcome by the electron. As a result, most diodes perform better when exposed to higher pulsed laser energy. [79, 80].

4. Conclusion

Using a pulsed laser, cubic shape and monoclinic shape of the Nano Hafnium oxide films were effectively prepared and deposited on substrates quartz. Higher laser energy was used to create blue shifts. With the laser energy, the average roughness values are rose and the values RMS are decreased. The FTIR and EDX measurements, Confirmed definitively obtaining nanostructures of HfO_2 through the appearance of the peaks of the active substances in the EDX tests (Hf, and O peaks), and the bonds of the active substances in the FTIR tests (H-0-F-O, and Hf-O bonds).The transmission is reduced with increased laser intensity due to an increase in hafnium dioxide grain concentration, finally the topographic are be more distributed with increasing the deposited laser energy as a result of enhanced the deposition rate and enhanced the growing Nano-film. The I-V test demonstrated that increasing the pulsed laser energies decreases the ideality-factor values while strengthening the (barrier-heights) and inverting the $Al/HfO_2/n$-Si diode's saturation current. The produced device demonstrates that HfO_2 is a versatile material for hetero-junction device production as a photodiode or solar cell, with a good rectification behavior and improved characteristics with the pulsed laser energies.

REFERENCES

[1] Cherkaoui, K., Monaghan, S., Negara, M. A., Modreanu, M., Hurley, P. K., O'Connell, D., McDonnell, S., Hughes, G., Wright, S., Barklie, R. C., Bailey, P., and Noakes, T. C. Q., Journal of Applied Physics, vol **104** (2008) p.064113.

[2] Karaduman, I., Barin, Ö., Özer, M., Acar, S., J. Electron. Mater. vol **45**, (2016) pp.3914-3920.

[3] Abood, M.K., Wahid, M.H.A., Saimon, J.A., Salim, E.T., International Journal of Nanoelectronics and Materials, vol **11(Special Issue BOND21)**, (2018) pp. 237-244.

[4] Robertson, J., High dielectric constant oxides, Eur. Phys. J. Appl. Phys., vol. **28**, (2004) pp. 265-291.

[5] Zhu, W.J., Tamagawa, T., Gibson, M., Furukawa, T., Ma, T.P., vol. **23**, Issue 11, (2002) pp. 649-651.

[6] Naayi, S.A., Hassan, A.I., Salim, E.T., International Journal of Nanoelectronics and Materials, vol. **11(Special Issue BOND21)**, (2018) pp. 1-6.

[7] Lin, S.-S., C.-S. Liao and S.-Y. Fan, Surface and Coatings Technology, vol. **271**, (2015) pp. 269-275.

[8] Wilk, G.D., Wallace, R.M., and Anthony, J.M., J. Appl. Phys, vol. **89**, (2001) pp. 5243-5275.

[9] Abood, M.K., Salim, E.T., Saimon, J.A., International Journal of Nanoelectronics and Materials, vol. **11(Special Issue BOND21)**, (2018) pp. 55-64.

[10] Martínez, F.L., Journal of Physics D: Applied Physics, vol. **40**, Issue 17, (2007) pp. 5256-5265.

[11] Lauria, A., Villa, I., Fasoli, M., Niederberger, M. & Vedda, A, ACS Nano, vol. **7**, (2013) pp. 7041–7052.

[12] Fakhri, M.A., Abdulwahhab, A.W., Dawood, M.A., Raheema, A.Q., Numan, N.H., Khalid, F.G., , Salim, E.T., International Journal of Nanoelectronics and Materials, vol. **11(Special Issue BOND21)**, (2018) pp. 103-108

[13] Wilk, G.D., R.M. Wallace, and J.M. Anthony, Journal of Applied Physics, vol. **89**, Issue 10, (2001) pp. 5243-5275.

[14] Jena, S., Tokas, R. B., Misal, J. S., Rao, K. D., Udupa, D. V., Thakur, S., Sahoo, N. K., Thin Solid Films, vol. **592**, (2015) p.135.

[15] Makram A. F., Evan T. S., Ahmed W. A., Hashim, U. Mohammed A M., Zaid T. S., Surface Review and Letters, vol. **26** issue 10, (2019) p. 1950068 11 pages.

[16] Golovchak, R., Shpotyuk, O., Kozdras, A., Vlček, M., Bureau, B., Kovalskiy, A., Jain, H., J. Phys.: Condens. Matter, vol. **20**, (2008) p. 245101.

[17] Knotek, P., Kutálek, P., Vlasová, M., Černošková, E., Janíček, P., Černošek, Z., Tichý, L., Mater. Chem. Phys., vol. **195**, (2017) p. 236.

[18] Muhsien, M. A., Salim, E. T., Al-Douri, Y., Sale, A. F., Agool, I. R., Applied Physics A: Materials Science and Processing, vol. **120**, Issue 2, (2015) pp.725-730.

[19] El-Denglawey, A., Makhlouf, M., Dongol, M., El-Nahass, M., Mater. J., Sci. -Mater. Electron., vol. **26**, (2015) p. 5603.

[20] El-Denglawey, A., Makhlouf, M., Dongol, M., J. Non-Cryst. Solids, vol. **449**, (2016) p. 34.

[21] Taleb, S. M., Fakhri, M. A., Adnan, S. A., Journal of Ovonic Research, vol. **15**, Issue 4, (2019) pp. 261 – 269.

[22] Alburaih, H., El-Denglawey, A., Results Phys., vol. **7**, (2017) p. 1010.

[23] Balasubramanian, K., Han, X., Guenther, K. H., Appl. Opt., vol. **32**, (1993) p. 5594.

[24] Badr, B.A., Mohammed, Q.Q., Numan, N.H., Fakhri, M.A., Abdul Wahhab, A.W., International Journal of Nanoelectronics and Materials, vol. **12** issue 3, (2019) pp. 283-290.

[25] Oliver, J. B., Kupinski, P., Rigatti, A. L., Schmid, A. W., Lambropoulos, J. C., Papernov, S., Kozlov, A., Smith, C., Hand, R. D., Opt. Express, vol. **20**, (2012) p. 16596.

[26] Lin, S.-S., Li, H.-R., Ceram. Int., vol. **39**, (2013) p. 7677.

[27] Bader, B.A., Numan, N.H., Khalid, F.G., Fakhri, M.A., Abdulwahhab, A.W., Journal of Ovonic Research, vol. **15**, Issue 2, (2019) pp. 127-133.

[28] Khoshman, J. M., Kordesch, M. E., Surf. Coat. Technol., vol. **201**, (2006) p. 3530.

[29] Oliver, J. B., Smith, C., Spaulding, J., Rigatti, A. L., Charles, B., Papernov, S., Taylor, B., Foster, J., Carr, C. W., Luthi, R., Hollingsworth, B., Cross, D., Opt. Mater. Express, vol. **6**, (2016) p. 2291.

[30] Fakhri, M. A., Abdulwahhab, A. W., Kadhim, S. M., Alwazni, M. S., Adnan, S. A., Materials Research Express, vol. **6**, Issue 2, (2018) p. 026429.

[31] D. Cangialosi, V. M. Boucher, A. Alegría, J. Colmenero, Soft Matter, vol. **9**, (2013) p. 8619.

[32] R. Golovchak, A. Kozdras, V. Balitska, O. Shpotyuk, J. Phys.: Condens. Matter, vol. **24**, (2012) p. 505106.

[33] Al-Douri, Y., Makram, A.F., Bouhemadou, A., Khenata, R., Ameri, M., Materials Chemistry and Physics, vol. **203**, (2018) pp. 243-248.

[34] Hacinliyan, A. S., Skarlatos, Y., Aybar, I. K., Aybar, O. O., Shpotyuk, O., Golovchak, R., Balitska, V., Kozdras, A., J. Non-Cryst. Solids, vol. **386**, (2014) p. 8.

[35] Jensen, M., Smedskjaer, M. M., Wang, W., Chen, G., Yue, Y., J. Non-Cryst. Solids, vol. **358**, (2012) p. 129.

[36] Ibraheam, A. S., Rzaij, J. M., Makram, A. F., Abdulwahhab, A. W., Materials Research Express, vol. **6** ssue 5, (2019) pp. 055916.

[37] S. Jena, R. B. Tokas, S. Thakur, N. K. Sahoo, Indian J. Phys., vol. **90**, (2016) pp. 951.

[38] Majhi, A., Dilliwar, M., Pradhan, P. C., Jena, S., Nayak, M., Singh, M. N., Udupa, D. V., Sahoo, N. K., J. Appl. Phys., vol. **124**, (2018) p. 115306.

[39] Abood, M. K., Wahid, M. H. A., Salim, E. T., Jehan, A. S., The European Physical Journal Conferences, vol. **162**, (2017) p. 01058.

[40] Tokas, R. B., Jena, S., Misal, J. S., Rao, K. D., Polaki, S. R., Pratap, C., Udupa, D. V., Thakur, S., Kumar, S., Sahoo, N. K., Thin Solid Films, vol. **645**, (2018) p. 290.

[41] Dey, P. P., Khare, A., J. Alloys Compd., vol. 706, (2017) p. 370.

[42] Hassen, H.H., Salim, E.T., Taha, J.M., Mahdi, R.O., Numan, N.H., Khalid, F.G., Fakhri, M.A., International Journal of Nanoelectronics and Materials, vol. **11(Special Issue BOND21)**, (2018) pp. 65-72

[43] Saiter, J. M., Arnoult, M., Grenet, J., Physica B, vol. **355**, (2005) p. 370.

[44] Jena, R. B. Tokas, S. Tripathi, K. D. Rao, D. V. Udupa, S. Thakur, N. K. Sahoo, J. Alloys Compd, vol. **771**, (2019) p. 373.

[45] Fakhri, M. A., Wahid, M. H. A., Badr, B. A., Salim, E. T., Hashim, U., and Salim, Z. T., The European Physical Journal Conferences, vol **162**, (2017) p. 01004.

[46] Naik, R., Jena, S., Ganesan, R., Sahoo, N. K., Phys. Status Solidi (B), vol. **251**, (2014) p. 661.

[47] González-Leal, J. M., Phys. Status Solidi (B), vol. **250**, (2013) p. 1044.

[48] Raid, A. I., Evan, T. S., Walid, K. H., Materials Science and Engineering C, vol. **33**, issue 1, (2013) pp. 47-52.

[49] Naik, R., Jena, S., Ganesan, R., Sahoo, N. K., Indian J. Phys., vol. **89**, (2015) p. 1031.

[50] Fakhri, M. A., Wahid, M. H. A., Kadhim, S. M., Badr, B. A., Salim, E. T., Hashim, U., and Salim, Z. T., The European Physical Journal Conferences **162** (2017) p. 01005.

[51] Abood, M. K., Salim, E. T., and Saimon, J. A., International Journal of Nanoelectronics and Materials, vol. **11**, issue 2 (2018) pp. 127-134.

[52] Gao, L., Zhou, L., Feng, J., Bai, L. & Liu, Z., Ceram. Int., vol. **38**, (2012) pp. 2305–2311.

[53] Manory, R. R., Mori, T., Shimizua, I., Miyake, S. & Kimmel, G., J. Vac. Sci. Technol. A, vol. **20**, (2002) pp. 549–554.

[54] Mohsin, M.H., Numan, N.H., Salim, E.T., Fakhri, M. A., Journal of Renewable Materials, vol. **9**, issue 9, (2021) pp.1519-1530

[55] Chen, G. H., Hou, Z. F., Gong, X. G. & Li, Q., J.Appl. Phys., vol. **104**, (2008) p. 074101.

[56] Jiang, C., Wang, F., Wu, N. & Liu, X., U Adv. Mater., vol. **20**, (2008) pp. 4826–4829.

[57] Salim, E.T., Khalid, F.G., Fakhri, M.A., Mahmood, R.S., Materials Today: Proceedings, vol. **42**, (2021) pp. 2422-2425.

[58] Fahrenkopf, N. M., Rice, P. Z., Bergkvist, M., Deskins, N. A. & Cady, N. C., ACS Appl. Mater. Interfaces, vol. **4**, (2012) pp. 5360–5368.

[59] Lu, C. H., Raitano, J. M., Khalid, S., Zhang, L. & Chan, S. W., J. Appl. Phys., vol. **103**, (2008) p. 124303.

[60] Basel, S., Numan, N. H., Khalid, F. G., Fakhri, M. A., AIP Conference Proceedings, vol. **2213**, issue 1, (2020) p. 020228.

[61] Jayaraman, V., Bhavesh, G., Chinnathambi, S., Ganesan, S. & Aruna, P., Mater. Express, vol. **4**, (2014) pp. 375–383.

[62] Quintero-García, J. S., Puente-Urbina, B. A., García-Cerda, L. A., Rodríguez-Fernández, O. S. & Mendoza-Mendoza, E. A., Mater. Lett., vol. **159**, (2015) pp. 520–524.

[63] Fakhri, M.A., Basheer, R.A., Banoosh, A.M., Azeez, H. N., Digest Journal of Nanomaterials and Biostructures,, vol. **16**, issue 2, (2021) pp. 367-375.

[64] Marwa, A. M., Evan, T. S., and Ibrahim, R. A., International Journal of Optics, vol. **2013**, (2013) Article ID 756402, 9 pages.

[65] Rauwel, P., Rauwel, E., Persson, C., Sunding, M. F. & Galeckas, A., J. Appl. Phys., vol. **112**, (2012) p. 104107.

[66] Hassan, M.A., Al-Nedawe, B.M., Fakhri, M.A., Applied Optics, vol. **60**, issue 8, (2021) pp. 2339-2347.

[67] Nahar, R. K., Vikram, S., Aparna, S., Journal of Materials Science: Materials in Electronics, vol. **18**, (2007) pp. 615–619.

[68] Raid, A. I., Evan, T. S., Halemah, T. H., (2021). Optik, vol. **245**, (2021) p. 167778.

[69] Hector, G., Helena, C., Salvador, D., Luis, B., Francesca, C., Journal of Vacuum Science & Technology A, vol. **31**, (2013) p. 01A127.

[70] Evan, T. S., Marwa, S. A., Makram, A. F., Modern Physics Letters B, vol. **27**, issue 16, (2013) p. 1350122.

[71] Gritsenko, V. A., Perevalov, T. V. & Islamov, D. R., Physics Reports, vol. **613**, (2016) pp. 1–20.

[72] Hassan, M. M., Fakhri, M. A., Adnan, S. A., Digest Journal of Nanomaterials and Biostructures, vol. **14**, issue 4, (2019) p. 873-878.

[73] Branko, M., Jelena, M., Jelena, L., Maria, Č., Svetlana, B., Ceramics International, vol. **42**, (2016) pp. 615–620

[74] Makram, A. F., Najwan, H. N., Qamar, Q. M., Mustafa, S. A., Omer, S. H., International Journal of Nanoelectronics and Materials, vol. **11 (Special Issue BOND21)**, (2018) pp. 109-114.

[75] Altındal, S., Dokme, I., Bulbu, M. M., Yalcın, N., Serin, T., Microelectronic Engineering, vol. **83**, (2006) pp. 499–505.

[76] Harishsenthil, P., Chandrasekaran, J., Marnadu, R., Balraju, P., Mahendran, C. Physica B: Condensed Matter, vol. **594**, (2020) pp. 412336.

[77] Badr, B. A., Mohammed, Q. Q., Numan, N. H., Fakhri, M. A., Abdulwahhab, A. W., International Journal of Nanoelectronics and Materials, vol. **12,** issue 3, (2019) pp. 283-290

[78] Liu, H., Dandan, Z., Shunrun, C., Jinwan, H., Dian, T., RSC Advances, vol. **5**, (2015) pp. 62891–62898.

[79] Chao, L., Tibor, J. H., David, K., Yunxia, J., Wei, H., Advanced Functional Materials, vol. **25** (2015) pp. 4607–4616.

[80] Fakhri, M. A., Al-Douri, Y., Bouhemadou, A., Ameri, M., Journal of Optical Communications, vil. **39**, issue 3, (2017) pp. 297-306